INTERNATIONAL JOURNAL OF HYDROGEN ENERGY 44 (2019) 12057–12072

Available online at www.sciencedirect.com

ScienceDirect

journal homepage: www.elsevier.com/locate/he

Ex situ characterization and modelling of fatigue crack propagation in catalyst coated membrane composites for fuel cell applications

Yadvinder Singh, Ramin M.H. Khorasany, Will H.J. Kim, Alireza Sadeghi Alavijeh, Erik Kjeang, R.K.N.D. Rajapakse, G. Gary Wang*

School of Mechatronic Systems Engineering, Simon Fraser University, 250-13450 102 Avenue, Surrey, BC, V3T 0A3, Canada

ARTICLE INFO

Article history:
Received 8 January 2019
Received in revised form
9 March 2019
Accepted 15 March 2019
Available online 9 April 2019

Keywords:
Fuel cell
Catalyst coated membrane
Durability
Crack propagation
Paris law
Fracture

ABSTRACT

Interactions between catalyst layers and membrane are known to influence the mechanical properties of catalyst coated membrane (CCM) composites used in fuel cells, and can further affect their fatigue-driven mechanical fracture — an important lifetime-limiting failure mode in automotive applications. Here, the fracture propagation phenomenon in CCMs is characterized through a series of *ex situ* experiments and microstructural investigations conducted across a range of stress, temperature (23-70 °C), and relative humidity (50–90%) conditions relevant to low-temperature polymer electrolyte fuel cells. In comparison to pure membranes, the crack propagation rates are slightly arrested in CCMs through mechanical reinforcement offered by the catalyst layers; however, the membrane layer still controls the overall crack growth trends through its temperature and humidity dependent ductile fracture characterized by confined yielding around the fracture surface. Local interfacial delamination and severe electrode cracking are found to accompany the CCM crack propagation, which aids membrane fracture by loss of local reinforcement. A Paris law based fracture modelling framework, incorporating the elastic-viscoplastic mechanical response of CCMs, is developed to semi-analytically evaluate one-dimensional crack growth rate during cyclic loading, and provides reasonably accurate predictions for the present *ex situ* problem.

© 2019 Hydrogen Energy Publications LLC. Published by Elsevier Ltd. All rights reserved.

Introduction

In recent decades, global environmental concerns related to greenhouse gas (GHG) emissions have promoted research and development efforts on sustainable and clean energy based power sources [1]. Among the potential alternatives are hydrogen-based polymer electrolyte membrane (PEM) fuel cell systems, particularly in the transportation sector that presently relies heavily on combustion of fossil fuels [2]. These systems generate electricity through an electrochemical conversion of hydrogen (fuel) and oxygen (oxidant) with water as a by-product, and can be used to power fuel cell electric vehicles (FCEVs) in a clean, noise-free, and efficient manner [3]. Large-scale commercial viability of this promising technology in automotive applications, however, requires further

* *Corresponding author.*
E-mail address: ekjeang@sfu.ca (E. Kjeang).
https://doi.org/10.1016/j.ijhydene.2019.03.108
0360-3199/© 2019 Hydrogen Energy Publications LLC. Published by Elsevier Ltd. All rights reserved.

cost reductions and durability enhancements. The multi-physical processes that enable fuel cell operation can degrade its components over time, typically leading to a gradual performance loss and eventual failure of the fuel cell.

Electrolytic membrane is an important functional component of the fuel cell that facilitates transport of protons between its opposite electrodes, while simultaneously acting as an electronic insulator and a physical barrier against combustive intermixing of the reactants. The solid-state membrane used in PEM fuel cells is typically made from perfluorosulfonic acid (PFSA) polymer [4]. Automotive duty cycles can introduce various degradations processes and damage modes within the PFSA membrane, *viz.* cracks, tears, pinholes, thinning, shorting, and delamination, thereby compromising its key functionalities and often contributing significantly toward the ultimate failure of the fuel cell system [5]. Operational membrane degradation comprises multiple, and often synergistic, chemical, mechanical, and thermal mechanisms [6–8]. Moreover, the intensity of these mechanisms may be spatially distributed within the cell due to local variations in conditions [9,10]. The chemical degradation mechanisms typically involve the generation of radical species that attack the membrane's molecular structure, and deteriorate its structural integrity and material properties [11–17]. In contrast, the mechanical degradation mechanisms are driven by mechanical stresses that develop within the membrane due to its assembly and constrained expansion/contraction under hygrothermal fluctuations [18–22], and are capable of inducing membrane failure through fatigue and/or creep phenomena. The chemical and mechanical stressors also have strong interactions [8,15,23–25] and are thermally sensitive [18,19,21,26–28], which can often accelerate the degradation rate. Given the highly coupled, and therefore complex, nature of membrane degradation and its strong impact on fuel cell durability, a wide range of research has addressed this topic comprising of fundamental studies on membrane's material behaviour characterization [19,21,26,29–39], accelerated stress testing (AST) [5–8,10,25,40–48], operational lifetime prediction [18,20,49–52], and strategies for degradation mitigation [53–58].

Crack development is as a dominant lifetime-limiting failure mode of fuel cell membranes, both during their mechanical or combined chemical/mechanical ASTs and field operation [5,10,15,45–48]. The membrane cracks typically result from its fracture under the impact of *in situ* mechanical stresses that develop during fuel cell operation [10,20,40]. Membrane durability against such failures is governed by its resistance to fracture, which can be characterized by measuring its intrinsic fracture energy [59]. The fracture process in polymeric materials, however, is often accompanied by viscous dissipation and plastic deformation that makes it challenging to decouple the fundamental fracture energy. Several techniques have been proposed for performing measurements that approach this intrinsic property, including the essential work of fracture (EWF) [59,60], trouser tear test [59,61], double cantilever beam test [61], and knife slit test [59,62], of which the latter is considered as the most promising. From a temporal standpoint, the development process of any individual crack, under fatigue and/or creep loading, can be broadly categorized into two stages — *crack initiation* followed by *crack propagation*. While the exact proportions of these two stages within the overall *in situ* lifetime are still debatable in literature and subject to further research, there is a general consensus on the importance of understanding, and thereby controlling, each stage to achieve enhanced membrane durability [18,19,63–66].

Focused fundamental studies aimed at characterizing the crack development process are typically carried out through *ex situ* experiments that employ standardized specimen geometries and controlled loading conditions. The initial experimental efforts mainly targeted the generation of *S–N* (stress–fatigue cycles) curves characterizing the overall fatigue fracture lifetime [18,19,49]. These studies reported the membrane or MEA fatigue lifetime to be exponentially related to applied mechanical stresses with strong dependence on temperature and humidity conditions. In additional to the conventional cyclic tensile testing, pressure-loaded blister testing has also been employed to characterize the fatigue lifetimes under repeated lateral bulge deformations [50,65]. Modelling studies for predicting the membrane fatigue lifetime under hygrothermal cycling were performed based on deformation energy [67] and Smith-Watson-Topper (SWT) criterion [52], respectively.

Isolated characterization of membrane crack propagation has been lately gaining attention of the fuel cell research community owing to its direct impact on overall fuel cell durability. Our group [26] recently characterized the average fatigue crack growth rates in non-reinforced *Nafion*® NR-211 membranes over a range of operationally relevant stress, temperature, and relative humidity (RH) conditions. The results demonstrated a strong sensitivity of the fatigue crack propagation behaviour to these conditions, especially temperature, and the predominantly ductile nature of membrane fracture accompanied by localized plastic deformation. Zhang et al. [63] examined crack propagation in *Nafion*® XL composite membranes, which are reinforced by an expanded polytetrafluoroethylene (ePTFE) layer in the middle, and found their fatigue crack growth behaviour to be highly anisotropic in-plane and sensitive to the orientation of ePTFE fibres. They further showed the effectiveness of reinforcement in slowing down the rate of crack propagation, which was attributed to a 'fibre bridging' effect offered by the mechanically tough ePTFE layer that offsets stress at the propagating crack tip through a local stress sharing mechanism. Lin et al. [64] explored the effects of biaxial loading conditions and reported that additional stresses parallel to the direction of crack growth can slow down the rate of crack propagation. While the branching effect in membrane cracks under *in situ* fuel cell conditions commonly requires chemically-induced material embrittlement [46–48], this work demonstrated the plausibility of crack branching under purely mechanical ductile fracture for specific *ex situ* cases of biaxial loading.

Modelling efforts on simulating the crack propagation behaviour in fuel cell membranes have been relatively numerous, particularly under *in situ* conditions involving RH cycling. Kusoglu and Weber [68] introduced a mechanistic theoretical framework for simulating the radial growth of circular pinholes within the plane of a simplified constrained membrane geometry during RH cycling. The model predicted that pinhole growth can be arrested by increasing the

clamping compression, and by increasing the material's yield strength and dimensional stability. Banan et al. [69–71] used finite element method (FEM) in conjunction with cohesive zone theory to study the individual and combined effects of mechanical vibrations and hygrothermal cycling, respectively, on the growth of interfacial delamination and membrane cracks. More recently, Ding et al. [72] developed a particularly elegant approach for modelling the *in situ* through-plane crack growth in fuel cell membranes by combining a plastic energy dissipation criterion with a node release algorithm in FEM, and demonstrated its efficacy in capturing key experimental observations such as the improved durability of reinforced membranes and faster crack propagation under the flow channels. While these modelling efforts have been reasonably effective in predicting various qualitative aspects of the *in situ* membrane crack propagation behaviour, their quantitative effectiveness has been limited, among other reasons, by a lack of relevant experimental data available on: (i) fundamental failure criterion used within the models [68,69,72]; and (ii) *in situ* crack growth rate measurements against which they could be directly validated. To partly circumvent these challenges, Singh et al. [26] implemented an empirically-inspired semi-analytical fracture modelling approach using the analytical relations of Paris law [73] and fracture mechanics for an elastic-viscoplastic material treatment, and were able to validate its reasonable quantitative accuracy for the case of uniaxial *ex situ* fatigue propagation in *Nafion*® NR-211 membranes, which can potentially be adapted further for *in situ* fuel cell applications.

The membrane is typically fused together with catalyst layers (CLs) on each side to form a composite catalyst coated membrane (CCM) before assembling it into the fuel cell. Mechanical and fatigue properties of the CCM as well as their relationships to temperature and humidity differ substantially from pure membrane, partly due to the mechanical reinforcement offered by the CLs [18,37]. Moreover, the hygral response of the membrane is constrained by the bonded CLs leading to lower stresses during hydration-dehydration cycles [39]. The implications of these fabrication-induced variations were clarified by Khorasany et al. [74] wherein the *in situ* stress profiles simulated within a fuel cell MEA during hygrothermal cycling were found to differ considerably based on the choice of pure membrane or CCM properties, respectively. Effect of CLs on the membrane crack propagation behaviour, however, still remains unexplored in the published literature [26,63,64].

The objective of the present work is to characterize fatigue-driven crack propagation in CCM composites, and compare against the corresponding data available for pure membranes [26] to ascertain the added effects of bonded CLs. The quantitative investigation involves *ex situ* experiments across a range of environmental and loading conditions that mimic the *in situ* fuel cell environment. The qualitative aspects are examined through a three-dimensional visual analysis of the structural and morphological changes that accompany CCM crack growth. Finally, a semi-analytical fracture modelling framework [26], which is based on Paris law and incorporates a time-, temperature-, and humidity-dependent elastic-viscoplastic constitutive material behaviour, is applied to simulate one-dimensional crack propagation rates within the plane of CCM composites under uniaxial cyclic mechanical loads.

Experimental procedure

Materials

Membrane electrode assemblies (MEAs) were first fabricated by hot-pressing a 25 μm thick non-reinforced *Nafion*® NR-211 perfluorosulfonic acid (PFSA) ionomer membrane between gas diffusion electrodes (GDEs) [10,14] based on a previously reported procedure [18,37,39]. The anode and cathode catalyst layers (CLs) of the GDEs were composed of carbon-supported Pt and PFSA ionomer. The catalyst coated membrane (CCM) composites used during the present experimental work were obtained by delaminating gas diffusion layers (GDLs) from the fabricated MEAs. In similarity with our previous work on pure membranes [26], double edge notch tension (DENT) specimens were prepared from rectangular CCM samples of 10 mm width and 20 mm gauge length. Initial cracks with 0.7 mm crack length (a_i) were artificially created on both edges of the specimen by using a custom-made die made from hardened steel blades. This cutting procedure maintained the variability across opposite edge crack lengths under 2%, thereby ensuring an adequate DENT specimen symmetry. The quality of the initial crack was additionally examined with an optical microscope prior to each experiment.

Crack propagation tests

Ex situ crack propagation experiments were performed on the CCM DENT specimens using a *TA Instruments Q800* dynamic mechanical analyzer (DMA) equipped with humidity control. The specimens were initially loaded in a tensile grip at room conditions under a small preload force of 0.001 N, and were then gradually brought to the desired experimental conditions of temperature and humidity while sustaining the preload. The specimens were further held at these experimental conditions for 30 min before testing to ensure adequate dimensional stabilization. Following the stabilization, the specimens were subjected to uniaxial cyclic tensile force applied longitudinally. The cyclic force was sinusoidal with 10 Hz frequency and minimum to maximum load ratio (*R*) of 0.2, which is consistent with our previously reported *ex situ* fatigue and fracture studies [18,19,26]. Experiments were carried out at four different combinations of temperature (23 °C and 70 °C) and relative humidity (50% and 90%) conditions, which are representative of their typical ranges in an operating automotive fuel cell [37]. Four different loading amplitudes, which produced a discernible crack propagation of about 30–40% of the initial crack length within a reasonable experimental timeframe, were examined at each test condition. The individual crack lengths (both left and right) were measured before and after each experiment using an optical microscope, and an average crack growth rate was thus determined using the incremental crack length and experiment duration. The experiments were repeated at least three times for each reported data point. Unless stated otherwise, the applied stress was calculated based on total specimen thickness inclusive of

the CLs and specimen width measured at the cross-section bearing the initial crack, *i.e.*, $10 - 2a_i$ mm. The maximum applied stress during the cyclic loading was always kept below the CCM yield strength (σ_Y) value reported by Goulet et al. [37] for each environmental condition, which ensured that the bulk stress levels within the CCM remained within the elastic regime such that the fatigue-driven crack propagation proceeded predominantly through a localized small-scale yielding process active near the crack tips [75].

X-ray computed tomography

The CCM is a layered composite structure fabricated from two materials with fundamentally distinct character — the *Nafion*® membrane is highly ductile experiencing significant plastic deformation prior to its failure [76] whereas the catalyst layer is relatively brittle [77]. When a through-thickness crack propagates within the plane of composite CCM, similar to the case of the present experiments, the individual layers can be expected to respond differently to local stress concentration effects which accompany the crack growth. For similar reasons, the response of individual layers to bulk mechanical loading in regions isolated from the crack-induced stress concentration may also be different. These differences in the mechanical response of individual layers within the CCM composite can be studied by analyzing their microstructural/morphological changes after being subjected to mechanical loading and the associated crack propagation pattern.

In the present work, microstructural investigation of selected CCM specimens utilized during the fracture experiments was conducted by analyzing 3D virtual images that were obtained from a laboratory-based X-ray computed tomography (XCT) microscope, *ZEISS Xradia VersaXRM-520*®. The CCM specimens to be imaged were fastened to a rigid plastic support using an adhesive tape to prevent sample movement during tomography acquisition. The plastic-supported specimens were placed on the rotation stage of the XCT system using a clip-type sample holder. The X-ray source was operated at 7 W power and 80 kV voltage without any filter. The rotation stage bearing the samples was placed at distances of 24 mm from the X-ray source and 30 mm from a 4X magnification detector, respectively, which resulted in a pixel resolution of nearly 1.5 μm. A total of 1601 projections were captured during a 360° sample rotation with 1 s exposure time per projection. Zeiss' proprietary *XMReconstructor*® software was then used to reconstruct the set of 2D projections acquired during tomography into a viewable 3D virtual image. The structural features of the acquired 3D data set were analyzed using *Avizo 3D*® (ver. 7.0) data visualization software. Additional details on the aforementioned XCT-based 3D analysis can be found in ref. [46].

Experimental results and discussion

Ex situ crack propagation rates

The average crack growth rates measured for the DENT CCM specimens when subjected to uniaxial cyclic tensile mechanical loading, as described in the previous section, are shown in Fig. 1 for both left and right side cracks. The growth rates are plotted against the amplitude of applied bulk stress ($\Delta\sigma$), which is the difference between the peak stress values of the adopted sinusoidal loading pattern. Measured data are shown across a range of temperature and relative humidity (RH) conditions that may be experienced by CCMs during actual fuel cell operation [37]. The cracks on either side of the DENT specimen appear to propagate at fairly symmetric rates and suggest similar trends with the variations in test conditions. The minor discrepancies observed might be due to microscale differences between the geometries of opposite cracks, and are well within the variability of the experimental measurements.

For both RH conditions examined, the crack propagation rates are significantly higher at the elevated temperature of 70 °C compared to the room temperature condition of 23 °C. While the crack propagation rates also increase with increasing RH from 50% to 90% at both examined temperatures, the effect of temperature change is clearly more pronounced compared to RH variations within the chosen range of test conditions. An increasing effect is also observed on the sensitivity of crack propagation to $\Delta\sigma$, which is represented by the slope of the data sets at each condition in Fig. 1. The sensitivity increases with both temperature and RH rise, again with the temperature causing a more dramatic increase.

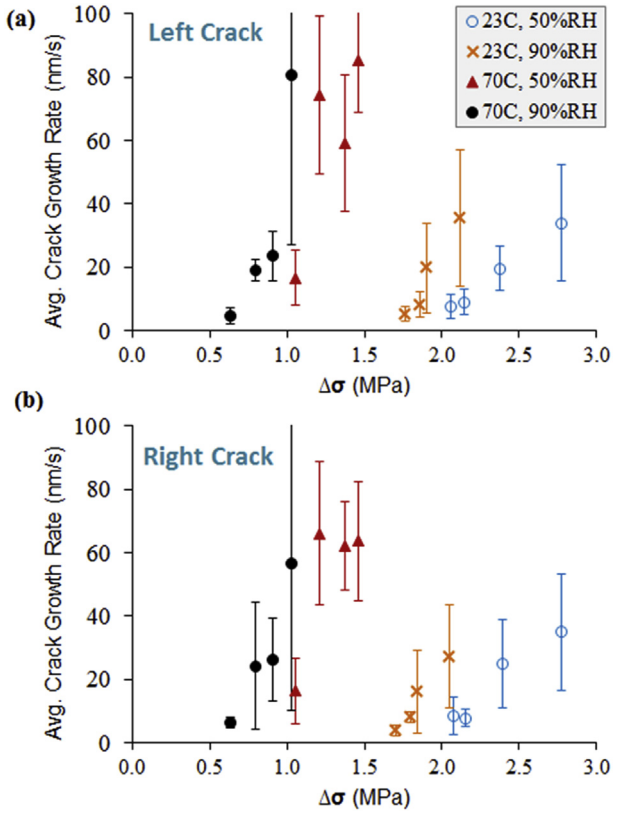

Fig. 1 – Average crack growth rates for: (a) left side crack; and (b) right side crack at various applied stress amplitudes ($\Delta\sigma$) and environmental conditions, as indicated. The error bars represent one standard deviation of the average value obtained from three measurements taken at each data point.

These observations suggest a reduced fracture resistance of the CCM composite at elevated temperature and RH conditions, and can be explained on the basis of fundamental mechanical properties. Goulet et al. [37] reported a decrease in both elastic modulus and yield strength of CCM with increasing temperature and RH. The temperature increase was also found to lower the post-yield strain hardening modulus in the plastic regime [37]. These deteriorations in the fundamental material properties at elevated temperature and RH conditions are expected to reduce the toughness of the CCM material, thereby compromising its resistance to fracture, thus leading to the faster crack propagation rates observed in the present work. Fig. 1 data also depicts that the crack propagation rate increases with increasing applied loading amplitude ($\Delta\sigma$) at any given environmental condition, which is likely caused by the associated increased amplitudes of mode-I stress intensity factor (K_I) during the cyclic fatigue loading [75]. The specimen elongation, which was additionally monitored during the experiments, was found to be lower than 2–3% of the initial length, indicating a predominantly elastic cyclic mechanical response throughout the bulk of the specimen, and with plastic deformations restricted mainly around the crack tip region that produced the observed fatigue crack growth.

A comparison of the fatigue crack propagation rates measured separately in the CCM composite and pure membrane, acquired from corresponding experiments performed using similar DENT sample geometries and fatigue loading profiles, is shown in Fig. 2 for two different environmental conditions: (i) 'room conditions' of 23 °C and 50% RH; and (ii) 'fuel cell conditions' of 70 °C and 90% RH [26]. The average propagation rates are plotted against the amplitudes of applied stress ($\Delta\sigma$) in Fig. 2a and applied force (ΔF) in Fig. 2b, respectively, wherein the stress is calculated using overall specimen thicknesses. The comparative results from Fig. 2a suggest a lower fracture resistance of the composite CCM than the pure membrane under both room and fuel cell conditions, with equivalent fatigue crack propagation rates observed at 2–3 times lower applied stress amplitudes. This result, however, seems counterintuitive given the favourable reinforcement effect of CLs on the membrane mechanical properties and associated fatigue stability that has been previously reported in literature [18,37,39]. This counterintuitive, and arguably misleading, result for comparative purposes stems from the definition of stress in Fig. 2a wherein the CLs and polymeric membrane within the CCM are implicitly assumed to carry equivalent stresses during the mechanical loading. This assumption, however, is fallible given that the CL material, which is highly porous and brittle with loosely constructed morphology, is fundamentally different from the ductile polymeric membrane. Unlike the membrane, the CLs often develop surface cracks during MEA fabrication [37,78], and additional cracks can readily develop within them under both static and cyclic tensile mechanical loading [77]. This premature CL crack development in the three-layer CCM composite structure, as observed during the present experiment, is shown in Fig. 2c. Accordingly, the individual contribution of the CLs to the overall mechanical response and/or fracture resistance of the CCM is most likely lower

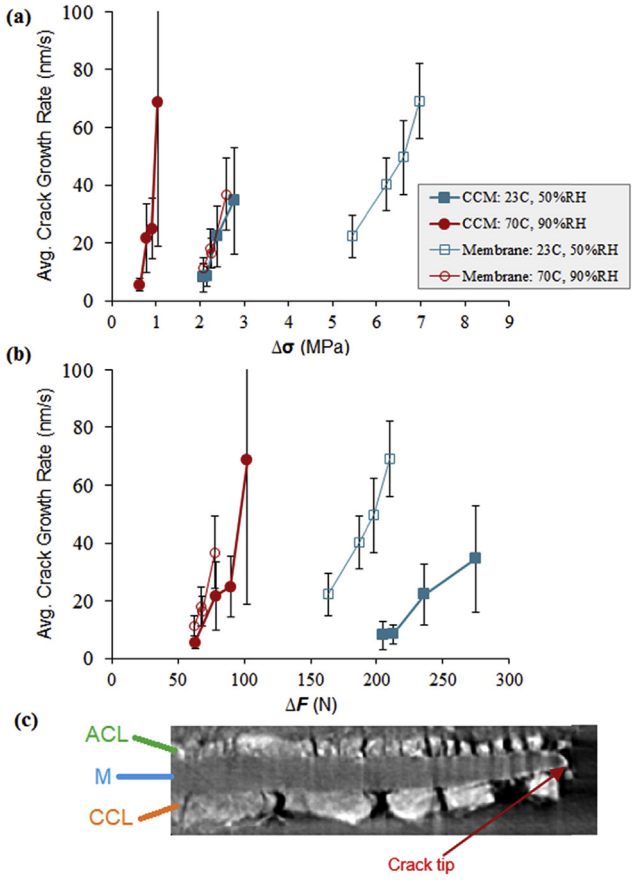

Fig. 2 – Comparison of average crack growth rates in CCM composite and pure membrane [26] as a function of: (a) applied stress amplitudes; and (b) applied force amplitudes. The stresses for the CCM data in (a) are evaluated based on total CCM thickness inclusive of the catalyst layers. Each data point represents combined measurement of left and right crack growth rates in the DENT specimen. (c) Cross-sectional image of the CCM, extracted from X-ray computed tomography data, showing its three-layer structure along with local membrane thinning at the crack tip and development of CL cracks. (ACL = anode catalyst layer; M = membrane; CCL = cathode catalyst layer).

than that of the membrane, and this difference is not adequately captured through the 'uniform' stress definitions of Fig. 2a.

A more robust and reliable comparison between the fatigue crack propagation behaviour of the CCM composite and pure membrane can be alternatively performed by considering the overall (applied) fatigue forces carried by the respective specimens, and is presented in Fig. 2b. Such a comparison may also be more representative of the *in situ* conditions wherein the in-plane forces that are generated within the MEA are primarily due to the membrane's constrained expansion/contraction under humidity fluctuations irrespective of the bonding quality with the adjacent CLs. With bonded CLs, the hygral expansion coefficient of the membrane is reduced within the CCM composite [74]; however, the individual

expansion/contraction of CLs and any associated contribution to in-plane forces is expected to be negligible based on the equivalent water sorption characteristics of pure membrane and CCM under similar hydration changes [39]. The comparative results shown in Fig. 2b, which are obtained by analyzing against the applied force amplitudes (ΔF), clearly demonstrate a higher resistance of the CCM composite against fracture growth compared to the pure membrane under both examined conditions. This behaviour is ascribed to the higher resistance of the CCM to elastic deformation and yielding compared to the pure membrane when subjected to similar tensile forces [37], and is generally consistent with the well-established knowledge around the favourable mechanical reinforcement effect of CLs on membrane within the CCM composites. Interestingly, the difference between the fatigue crack propagation behaviour in the two materials is more significant at room conditions than at fuel cell conditions while the CCM sustains its generally higher resistance to fracture growth (*cf*. Fig. 2b). This trend is also consistent with the findings of Goulet et al. [37] wherein they had shown a reduced difference in the effective mechanical stiffness and strength between CCM and pure membrane at elevated temperature and RH conditions. These findings further reaffirm the strong dependence of fatigue crack propagation behaviour on the fundamental mechanical properties of materials, and should thus encourage the development of predictive fracture models based on these properties such as the one presented later in this work.

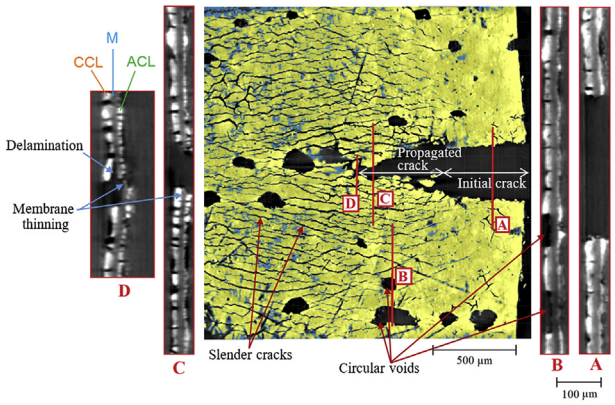

Fig. 3 – Planar top-down view of the cathode catalyst layer side of the CCM composite showing the fracture growth region (right side only) obtained after subjecting a CCM DENT specimen bearing initial edge cracks to cyclic tensile loading. The planar view is obtained from 3D virtual images generated through X-ray computed tomography, and with the data manually segmented into catalyst layer (yellow), membrane (blue), and void (black) phases for visual clarity. Cross-sectional views of selected locations are provided in the inset. (ACL = anode catalyst layer; M = membrane; CCL = cathode catalyst layer; and (For interpretation of the references to colour in this figure legend, the reader is referred to the Web version of this article.).

Microstructural investigation

Three-dimensional (3D) microstructural investigation is performed on the CCM specimens following their *ex situ* crack propagation tests by using virtually reconstructed morphological data sets obtained from XCT imaging. This 3D nature of microstructural analysis offers enhanced perspectives for damage examination whereby internal features of multilayered specimens, such as CCMs, can be non-invasively visualized in their natural state without disassembling the layer structure [46–48]. Fig. 3 shows a planar view of the cathode CL for one of the CCM DENT specimens subjected to cyclic tensile loading that resulted in propagation of the initial crack. As stated earlier, the initial crack is seen to have propagated in its original orientation under the influence of perpendicularly applied uniaxial cyclic mechanical loads. Two distinct types of surface defects, *viz*. slender cracks and circular voids as identified in Fig. 3, are observed in the cathode CL of the DENT specimen following this loading. The slender cracks are densely concentrated around the propagating crack and are absent in the region surrounding the initial crack, which is likely to be an under-stressed region due to the localized 'free' boundary conditions created by the pre-existing initial crack. The geometry and orientation of slender cracks further resembles the surface cracks typically reported for CCMs during uniaxial tensile test experiments [37,77,79]. The cross-sectional views shown in the inset of Fig. 3 that are taken within the region of the propagated crack (sections C and D) indicate the presence of localized membrane thinning, which is most severe in the vicinity of the crack surface and reduces with the distance from it. This observation is attributed to the confined yielding or plastic deformations occurring near the tip of propagating cracks during fatigue loading, and has also been previously observed for pure PFSA membranes [26,63]. Such localized membrane thinning is not observed around the surface of the initial crack (section A in Fig. 3), which was generated by cutting instead of fatigue driven propagation. Moreover, the membrane did not experience any discernible local thinning away from the crack tip where the CL cracks were present (Fig. 2c), which further suggests that the yielding of membrane was predominantly confined to the crack tip region only.

Zhang et al. [63] recently reported fatigue crack propagation experiments and microstructural investigation of *Nafion*® XL composite membranes, which consist of an ePTFE reinforcement layer between two PFSA layers. They showed that the crack propagation predominantly occurs in the outer PFSA layers of the membrane while the ePTFE fibres remain intact in the wake of the propagating crack, thereby providing resistance to crack propagation through a local stress sharing effect, also known as 'fibre bridging' [80]. They also observed interfacial delamination in this region and attributed it to the cyclic shear stresses that accompany this stress sharing phenomenon. Despite fundamental differences in the nature of participating materials, the multilayered CCM composites of the present work and the core-reinforced *Nafion*® XL membranes may be geometrically comparable given that the strongest layer within each composite is located at the center. The brittle outer layers of the CCM (*i.e.*, CLs) readily break with the

cyclic deformations of the inner membrane resulting in multiple slender cracks identified in Fig. 3; however, such scattered surface cracking was not apparent in front of the propagating crack in the outer PFSA layers of *Nafion*® XL membranes in ref. [63], which is likely due to the comparable mechanical response of all the layers to the fatigue loading. Moreover, no fibre formation is seen in the wake of the propagating crack within the CCM (*cf.* main figure and sections C and D in Fig. 3), thereby suggesting a limited role of the fibre bridging phenomenon in restraining the overall crack growth. However, delamination between the membrane and CL is observed in the wake region in the immediate vicinity of the membrane crack tip (*cf.* section D in Fig. 3), which is likely due to the locally concentrated crack tip opening displacement that may create intensified shear stresses resulting in such delamination effects. In contrast to the *Nafion*® XL composite membranes, the predominant monolithic crack propagation in CCM composites appears to be occurring within the inner membrane layer while the associated defects, such as delamination and CL surface cracks, work to nullify the otherwise present reinforcing role of the outer CL in the crack front region, thereby creating under-reinforced zones into which the membrane crack tends to propagate. Furthermore, the membrane and CL portions of the main propagating crack are observed to have the same planar geometry, indicating that the CL crack shape closely follows the underlying shape of the propagating crack in the membrane, provided that the membrane is the main load bearing part of the CCM. It should be noted that the above comparison between CCM composites and core-reinforced membranes is only intended to elucidate the variety of structural defects developing in these multilayered materials used in fuel cell MEAs; however, a more direct comparison with the present work would require crack propagation studies on CCM with reinforced membrane, which are presently unavailable in literature.

To further examine the various contributing factors in the development of surface CL cracks, a separate experiment is conducted by subjecting a CCM specimen having no initial edge cracks (*i.e.*, not a DENT specimen) to similar loading conditions and cycles as those employed during the fatigue crack propagation tests. This experiment represents a case of pure fatigue without any associated crack propagation. Additionally, the cathode CL plane is examined for a CCM DENT specimen that is not subjected to any cyclic loading. The planar view of the cathode CL of these two specimen is shown in Fig. 4. The slender crack features, which were observed around the propagated crack in Fig. 3, are also found in the cathode CL of the CCM specimen that had only experienced pure fatigue (Fig. 4a). Moreover, these features are absent in the non-cycled DENT specimen (Fig. 4b), thereby suggesting that the cyclic tensile fatigue loading is required to generate such slender CL cracks, both with and without any associated edge crack propagation. Interestingly, the density of these slender crack features around the propagated crack (Fig. 3) is more severe than that observed for the case of pure fatigue loading (Fig. 4a), while their orientations are generally comparable. This severe deterioration of the CL's structural integrity around a propagating through-thickness CCM crack is ascribed to the strong stress concentration effects that accompany crack propagation, as revealed by numerical simulations (discussed later).

Formation of void features with a somewhat circular in-plane geometry, which is different from the aforementioned sharp slender cracks, was another distinct form of damage observed on the cathode CL surface of the DENT specimens following cyclic loading (Fig. 3). Unlike the slender cracks that are densely concentrated around the propagated crack and its crack front, these circular voids are more randomly

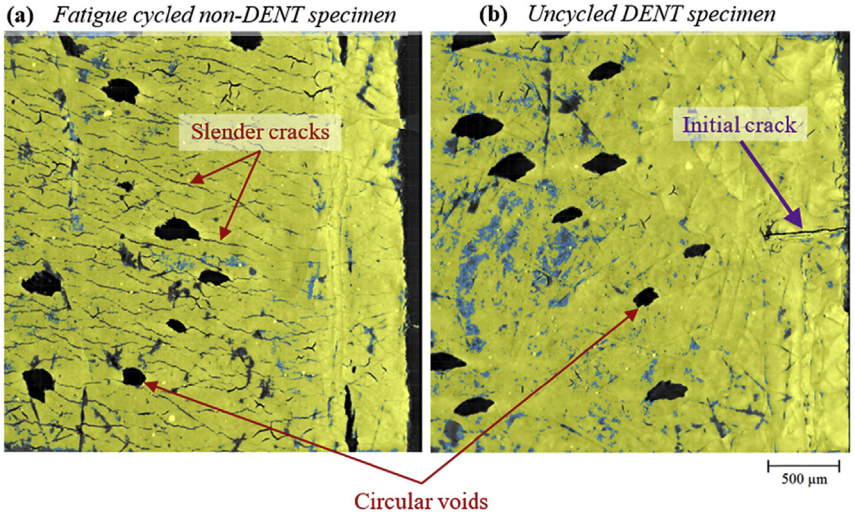

Fig. 4 – Planar top-down view of the cathode catalyst layer (right side only) of: (a) CCM specimen without initial edge cracks after being subjected to cyclic tensile loading; and (b) CCM DENT specimen bearing initial edge cracks but not subjected to cyclic tensile loading. The planar views are obtained from 3D virtual images generated through X-ray computed tomography, and with the data manually segmented into catalyst layer (yellow), membrane (blue), and void (black) phases for visual clarity. (For interpretation of the references to colour in this figure legend, the reader is referred to the Web version of this article.).

distributed across the CL surface and are even seen to develop in the under-stressed regions surrounding the initial crack. Such circular features having comparable geometry and sizes, however, can also be seen in the non-cycled DENT specimen (Fig. 4b) as well as the pure fatigue specimen (Fig. 4a), and accordingly, the present results may be insufficient to strictly correlate the development of these defects to fatigue and/or crack propagation. Instead, the circular voids observed in the present work represent sizeable chunks of missing electrode material, and are likely connected to the adopted sample preparation process involving a GDL delamination step (*cf.* 'Materials' section). As seen in Fig. 3 (section B), no discernible membrane thinning is observed adjacent to these circular voids, which further rules out any localized membrane yielding to be associated with their development. Nevertheless, the plausibility of the development of such CL void features under mechanical fatigue loads cannot be completely ruled out. This is because cyclic stresses are known to promote interfacial membrane—CL delamination [10,70], which may knock off small pieces of CL and create such defect geometries during *ex situ* experiments wherein the otherwise overlapping gas diffusion layers (GDLs) are absent. Exploration of these possibilities is not directly within the scope of this work but may be pursued in future studies, preferably by utilizing CCMs with reduced CL void densities.

Fracture model

The applied loading conditions and microstructural investigations of the *ex situ* crack propagation experiments described in the previous sections suggest a fatigue-driven crack growth in CCMs, wherein the crack tip experiences confined plasticity and is gradually propagated when subjected to cyclic tensile stresses. Our previous work [26] demonstrated the efficacy of Paris law theory [73] in obtaining accurate predictions of such fatigue-driven crack growth behaviour for pure membrane material. Although the composite CCM, which additionally consists of porous and brittle CLs, may structurally differ from a pure membrane, the nature of its mechanical response to tensile loading is nevertheless qualitatively similar to that of the pure membrane [37]. Moreover, the aforementioned observations of secondary surface cracking in the CLs indicate that the crack propagation behaviour of CCMs is predominantly governed by the membrane's fracture properties. Accordingly, the applicability of Paris law theory and associated modelling frameworks [26] in predicting fatigue crack propagation in CCMs is promising, and is therefore addressed in the following sections. This fracture modelling approach is implemented by first modelling the time-, temperature-, and humidity-dependent elastic-viscoplastic constitutive mechanical behaviour of CCM composites in *COMSOL Multiphysics*® version 4.3. This characteristic material behaviour is then imported into a separate finite element method (FEM) model representative of the DENT specimens used during the *ex situ* crack propagation experiments. Incremental crack propagation is thereafter simulated by combining numerical information from the FEM model and empirical data from the experiments, respectively, using analytical fracture mechanics formulations and the Paris law. The following sub-sections describe these models in detail along with the simulated results.

Elastic-viscoplastic constitutive model

Experimental studies have shown that the mechanical response of CCM composites follows a time-, temperature-, and humidity-dependent elastic-viscoplastic constitutive behaviour (*i.e.*, stress-strain relationship) comprising of: (i) initial linear elastic (or *Hookean*) regime; (ii) gradual rollover yielding; and (iii) plastic regime with strain hardening [37]. While this constitutive behaviour is qualitatively comparable to that of the pure membrane material and underscores the dominant influence of the membrane layer on the overall mechanics of the CCM, considerable quantitative differences still exist in the CCM's response [37,39] that may affect any extended fatigue or fracture predictions obtained from this response. In our previous work, an elastic-viscoplastic constitutive model capable of simulating the aforementioned mechanical response characteristics was developed for pure *Nafion*® NR-211 membrane material [26]. The constitutive model represented well-established physical models which consider the ionomer membrane structure to be a molecular network with interconnected molecular chains, and wherein the stress response is comprised of simultaneously active intermolecular and network mechanisms, respectively [35,74,81,82]. In the present work, the elastic-viscoplastic mechanical response of CCM composites is further simulated through a similar constitutive model developed in *COMSOL Multiphysics*® FEM software. The underlying theoretical formulations and FEM specifications remain similar to our previous work on pure membranes [26], wherein they were presented with comprehensive detail and therefore, are not repeated here for the sake of brevity. In the constitutive model, the CCM composite is treated as a single object and assumed to have uniform effective material properties without distinguishing between the individual membrane and catalyst layers. These effective material properties, which are required as inputs for the present CCM specific model, are taken from Refs. [37,74].

Fig. 5 compares the simulated mechanical response, *i.e.*, uniaxial tensile stress-strain data, of the CCM composite with the corresponding experimental tensile testing results reported by Goulet et al. [37]. The comparative results are presented for all combinations of temperature and RH that were chosen during the *ex situ* crack propagation experiments described in the previous sections, and are obtained from a uniaxial tensile test (simulated and experimental, respectively) conducted on a rectangular 10 mm × 2 mm CCM specimen at a constant strain rate of 0.0001 s^{-1}. The simulated results are found to have a good agreement with the experimental data across all examined conditions, thereby confirming the capability of the developed elastic-viscoplastic constitutive model to accurately simulate the CCM composite's mechanical response up to 100% strain levels. Moreover, the aforementioned qualitative aspects of the CCM's mechanical response are reasonably well captured by the model across the elastic, rollover yield, and plastic regimes. A discernible decrease in both elastic modulus and yield strength is apparent with increasing temperature and/or humidity. Moreover, the

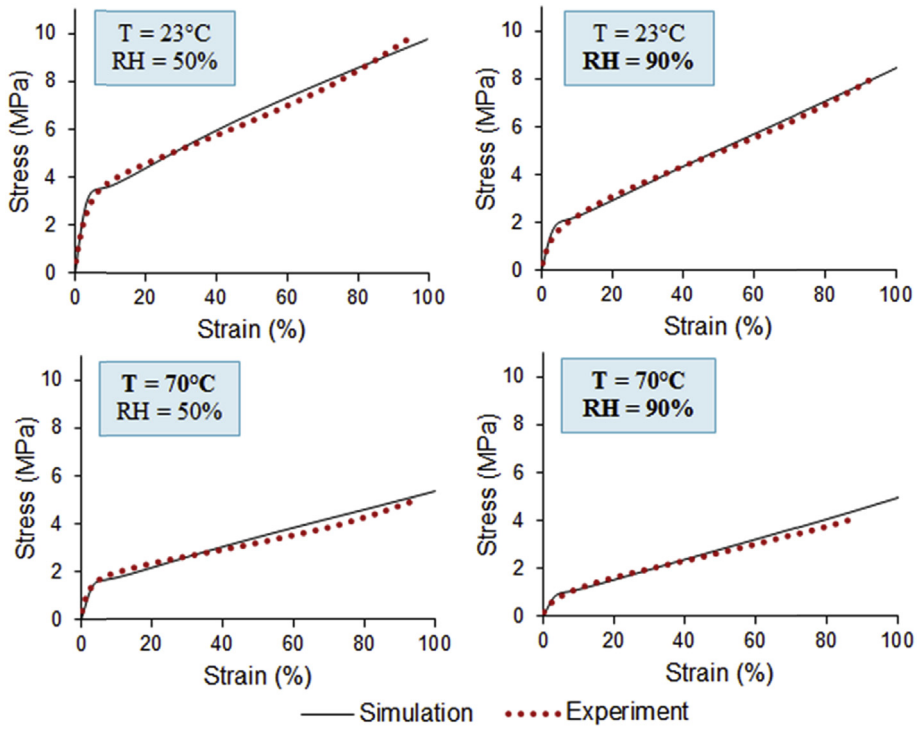

Fig. 5 – Comparison of experimentally characterized [37] and numerically simulated stress-strain data for the CCM composite material obtained at different temperature (T) and relative humidity (RH) conditions under uniaxial tensile loading performed at a constant strain rate of 0.0001 s^{-1}.

strain hardening effect that accompanies plastic deformation decreases in magnitude at an elevated temperature, as seen from the reduced slopes within the plastic regime. Similar agreements between the numerically simulated and experimental responses were also attained at higher strain rates owing to the incorporation of time-dependency in the CCM's elastic-viscoplastic constitutive model. Inclusion of this time-dependent behaviour is particularly suitable for fatigue loading scenarios where the strain-rate could change temporally, as well as the fracture simulations where it may also be spatially inhomogeneous. As noted previously during the discussion of the *ex situ* crack propagation experimental results, the variations in environmental conditions can severely alter the crack growth rates in the CCM composite, and the CCM's resistance to fracture is closely associated with its fundamental mechanical properties. Accordingly, the robust predictive capability demonstrated by the elastic-viscoplastic constitutive model in simulating the CCM's mechanical response (*cf.* Fig. 5) is of significance, and is critical to the model implementation within the overall fracture modelling framework for obtaining reliable predictive tools for the dependent crack propagation behaviour.

Semi-analytical crack propagation model

Paris law provides a convenient, and hence typically adopted, analytical expression for quantifying the fatigue-induced crack propagation behaviour in ductile materials, wherein the crack growth is driven by confined plastic deformations (or small-scale yielding) around the crack tip while the bulk material experiences cyclic elastic stresses [73]. For mode-I type of crack growth, which is representative of the experiments conducted in the present work using DENT specimens, the rate of crack propagation $\left(\frac{da}{dN}\right)$ is related to the cyclic amplitude of the applied stress intensity factor (ΔK) as follows

$$\frac{da}{dN} = C(\Delta K)^m \tag{1}$$

where a is the instantaneous crack length after N fatigue loading cycles, and C and m are material parameters related to its resistance to fatigue-driven crack growth and are further dependent on temperature and humidity conditions [70].

The stress intensity factor (K), which is the driving force for crack growth as per the Paris law expression of Eq. (1), accounts for the combined effects of applied load and crack/specimen geometry on the crack propagation rates, and its amplitude during cyclic loading can be expressed as

$$\Delta K = \Delta\sigma.\sqrt{\pi a}.C_c \tag{2}$$

where $\Delta\sigma = \sigma_{max} - \sigma_{min}$ is the variation in bulk or far-field tensile stress levels applied during each cycle, and C_c is the configuration correction factor whose value depends upon the specimen geometry and nature of loading [83]. C_c is typically a non-linearly decreasing function of the instantaneous crack length, and mathematical formulations of this relationship for the small-scale yielding problems can be found in standard mechanical testing handbooks such as ref. [84]. Despite the prevalence of the small-scale yielding condition within the plane of the specimen during the fatigue crack propagation

experiments reported herein, the present work utilized very thin CCM specimens wherein the specimen thickness can be comparable to the size of the confined plastic zone surrounding the crack tip [20]. Accordingly, these standard formulations of $C_c(a)$ may not be directly applicable for evaluating ΔK values from Eq. (2) and subsequently using those values for generating the Paris curves as per Eq. (1). To overcome this challenge, J-integrals are numerically evaluated using a simulated FEM model of the experimental CCM specimen under corresponding loading and environmental conditions, and are utilized to approximate the stress intensity factor (K) values using the following relationship for isotropic linear elastic materials under plane stress assumption [85,86].

$$J = \frac{K^2}{E} \tag{3}$$

where E is the Young's modulus of elasticity. The amplitude ΔK is obtained from the J-integrals evaluated at the applied far-field tensile stress levels of σ_{max} and σ_{min}, respectively, using Eq. (3). The numerically simulated ΔK values enable the generation of experimental Paris curves along with the indirect numerical formulations of $C_c(a)$ relationships specific to the present work involving thin CCMs, both of which further aid in the evaluation of crack growth rates as per the Paris law given by Eq. (1). Further details on this semi-analytical crack propagation modelling approach can be found in our previous work reported for pure membranes [26].

In accordance with the specimen geometry and loading conditions of the *ex situ* crack propagation experiments described earlier, the FEM model of CCM DENT specimens is implemented in *COMSOL Multiphysics*® to simulate their mechanical response under uniaxial tensile loads. Given the specimen symmetry, only the left-half of the experimental DENT specimens is modelled, as shown in Fig. 6. A total of 1200 *3-node triangular plane stress* elements are used to mesh the modelled geometry along with a high mesh density around the crack tip, which enables high resolution characterization of the mechanical response within this region. Moreover, the previously described and validated elastic-viscoplastic constitutive response of the CCM composite material is incorporated into this FEM model, thereby ensuring realistic and therefore accurate simulations of this specific problem.

For each data point examined during the experiments, mechanical responses from the FEM model are characterized at incremental variations of 0.1 mm crack length starting from the initial crack length (a_i) of 0.7 mm up to the final crack length encountered in each case. Fig. 6 shows an example of this characterization wherein the distribution of first principal stress (σ_1) within the DENT specimen is simulated at crack lengths of 0.7 mm and

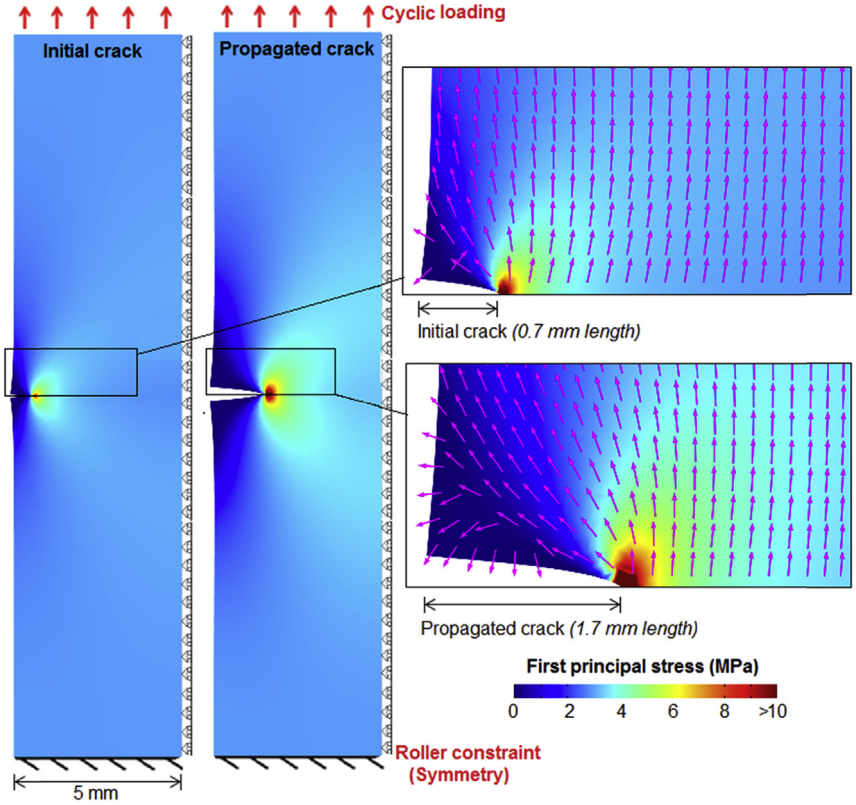

Fig. 6 – Finite element method (FEM) simulation of the distribution of first principal stress (σ_1) within the plane of CCM DENT specimens when subjected to a perpendicularly applied uniaxial tensile stress of 2.95 MPa at 23 °C and 50% RH. The stress states are shown at two different crack lengths, *viz.* 0.7 mm 'initial crack' and 1.7 mm 'propagated crack', respectively. Magnified views of the crack tip region are provided in the insets along with local orientations of σ_1 (shown by arrows). Due to specimen symmetry, only the left half of the DENT specimen is modelled.

1.7 mm, respectively, under an applied tensile stress of 2.95 MPa at 23 °C and 50% RH. Concentration of stresses can be clearly seen in the crack front region of the simulated specimen, which facilitates the preferential opening of new crack surfaces within this region under continued cyclic loading and thereby results in almost perfectly horizontal crack propagation along the direction of the initial crack (*cf.* Fig. 3). Moreover, the stress concentration effect is found to intensify at the higher crack length (see 'propagated crack' in Fig. 6) and can be expected to accelerate the instantaneous growth rates during crack propagation, similar to that reported by Kusoglu et al. [68] and Ding et al. [72], respectively, in separate simulation studies on non-reinforced PFSA ionomer membranes. The stress distribution shown in Fig. 6 also correlates with some of the microstructural findings described earlier. For example, the wake region behind the initial crack in Fig. 6 is relatively under-stressed and remains so during crack propagation, which is likely the reason behind the observed absence of slender cracks on the CL surface within this region (*cf.* Fig. 3). Instead, these slender CL cracks populate densely in front of and around the crack tip region, thus correlating well with the stress concentration regions simulated in Fig. 6. The magnified insets of Fig. 6 also show the local orientations of σ_1, which are not perfectly vertical but slightly tilted in the direction of crack propagation in the crack front region. This minor departure of local stress orientations from the applied bulk loading direction may have influenced the general orientation of the slender CL cracks, which is also not perfectly aligned with the crack propagation direction (*cf.* Fig. 3).

The simulation-based incremental characterization of the mechanical response of the CCM DENT specimen allows for mathematical relationships to be established between the configuration correction factor and instantaneous crack lengths, *i.e.*, $C_c(a)$, through the evaluated J-integrals and Eqs. (1)–(3). The obtained relationships are depicted in Fig. 7a for the room conditions (23 °C and 50% RH) and fuel cell conditions (70 °C and 90% RH) of the *ex situ* crack propagation experiments described earlier. At both conditions, $C_c(a)$ is found be a non-linearly decreasing polynomial function of the instantaneous crack length (a), as theoretically expected [26]. Moreover, slight differences in the C_c values are found to exist between the two environmental conditions, in particular at the lower crack lengths. These differences are attributed to the variations in the DENT specimen's stress-strain profiles (and the related J-integrals) that may occur between the two conditions due to the strong hygrothermal dependency of the CCM's mechanical response, as indicated in Fig. 5. Given that the C_c values are directly related to ΔK as per Eq. (2), and the crack propagation rate is quantified by Paris law as a mth power ($m > 4$ typically) of ΔK as per Eq. (1), these otherwise minor differences in C_c, if unaccounted for, may amplify errors in the crack propagation rates simulated by predictive models. Accordingly, the present work incorporates the numerically obtained $C_c(a)$ relationships that are specific to each test condition in order to minimize errors in quantitative predictions. For similar reasons, such condition-specific approaches may be further useful while applying the present methodologies to *in situ* crack propagation simulations where: (i) the temperature and/or RH fluctuate with time; and (ii) lower crack lengths (compared to those in Fig. 7a) may exist [46].

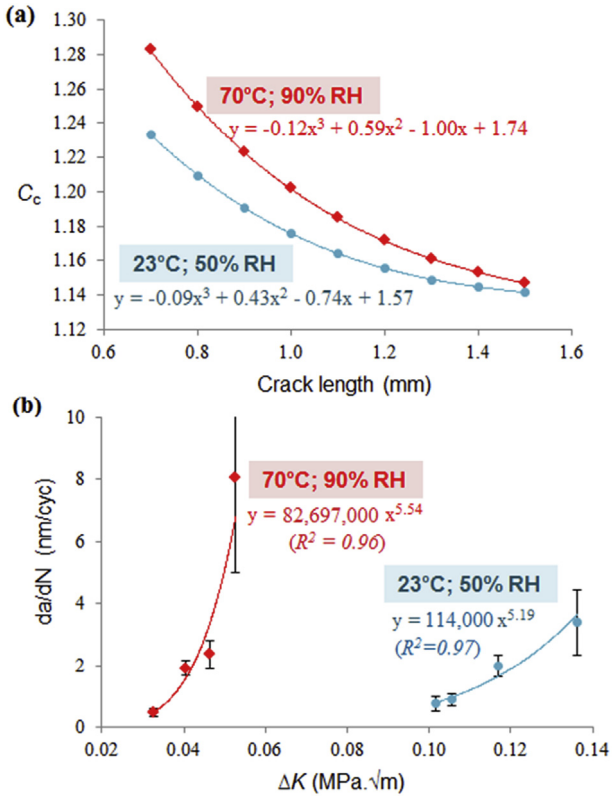

Fig. 7 – Fracture modelling of the CCM DENT specimen: (a) relationships between configuration correction factor (C_c) and crack length simulated from the FEM model wherein the symbols represent each incremental crack length chosen for the simulation; and (b) Paris curves between experimentally measured crack growth rate (da/dN) and simulated stress intensity factor (ΔK) wherein the symbols represent experimental data points. In both (a) and (b), results are shown at room conditions (23 °C and 50% RH) and fuel cell conditions (70 °C and 90% RH), and the trendlines shown are curve fitted to the data points for obtaining the corresponding mathematical expressions.

With $C_c(a)$ relationships established from the FEM simulations, ΔK values corresponding to each experimental data point are evaluated as per Eq. (2), and Paris curves are plotted between the experimentally obtained crack propagation rates $\left(\frac{da}{dN}\right)$ measured in nm per cycle and the simulated amplitude of the corresponding stress intensity factor (ΔK) measured in MPa.$\sqrt{m}$, as shown in Fig. 7b. The mathematical power law expression of the Paris curves yields Paris law parameter values of $C \approx 114{,}000$ and $m = 5.19$ at room conditions, and $C \approx 82,697,000$ and $m = 5.54$ at fuel cell conditions, respectively. These mathematical expressions have high coefficient of determination (R^2) with the data points at each condition (*cf.* Fig. 7b), thereby confirming that the mathematical fits along with the parameters deduced from them are sufficiently

accurate. The relatively higher magnitudes of both C and m parameters deduced at the fuel cell conditions are representative of the CCM composite's lower resistance to fracture growth at these conditions, which was also observed in the *ex situ* experimental results. These condition-specific parameters can now be utilized to integrate Eq. (1) such that the number of fatigue cycles required for extending a given crack between two known crack lengths can be evaluated.

Fig. 8 shows the number of cycles obtained by integrating the Paris law equation, *i.e.*, Eq. (1), between the corresponding initial and final crack lengths, and by utilizing the numerically evaluated condition-specific C and m parameters and $C_c(a)$ relationships across various test cases examined during the *ex situ* crack propagation experiments conducted on CCM DENT specimens. The experimentally applied number of cycles are also shown alongside for comparison. Within the experimental errors, which can be rather large for fracture phenomena as depicted by the error bars in Fig. 8, the number of cycles predicted through the Paris law based calculation are in acceptable agreement with the experiments across a range of temperature (23-70 °C) and humidity (50–90%) conditions that may be experienced by the CCM during typical fuel cell operation [37]. This validation establishes the capability of the semi-analytical crack propagation modelling framework adopted in this work to quantitatively simulate the mode-I type fracture propagation phenomenon in CCM composites during cyclic mechanical (or fatigue) stresses. Moreover, this modelling framework's efficacy has also been separately established for the case of pure membrane material (*i.e.*, without any bonded electrodes) in our previous work [26]. Similar cyclic fatigue stresses are known to develop within the plane of membrane/CCM under *in situ* conditions of fuel cell operation due to dynamic hygrothermal fluctuations [20,40,68,72,74]. In extreme cases, these *in situ* stresses have also been predicted to induce bulk plastic deformation within the membrane [20]. The modelling framework presented herein can potentially be adapted further to simulate *in situ* crack propagation rates during such operational fatigue stresses, which can be separately acquired using FEM [20,40,72,74,87,88], at least for the cases involving bulk elastic deformations and localized plasticity. Khorasany et al. [74] have shown that the simulated *in situ* stress profiles generated within a fuel cell MEA during hygrothermal cycling can differ considerably depending on the treatment of the CCM as: (i) a composite material with its exclusive material properties; or (ii) separate multiple layers of membrane and CLs having their individual properties. This choice of CCM treatment during *in situ* modelling would typically be guided by the lamination quality of the membrane—CL interfaces, which may further depend upon MEA design and fabrication procedures (*e.g.*, electrode coating process and hot pressing) as well as its degradation history. In general, the CCM composite treatment is expected to be favourable for in-plane crack propagation simulations, given that the CL and membrane components are normally bonded through the common ionomer phase after fuel cell conditioning (break-in). Nevertheless, the effectiveness of the semi-

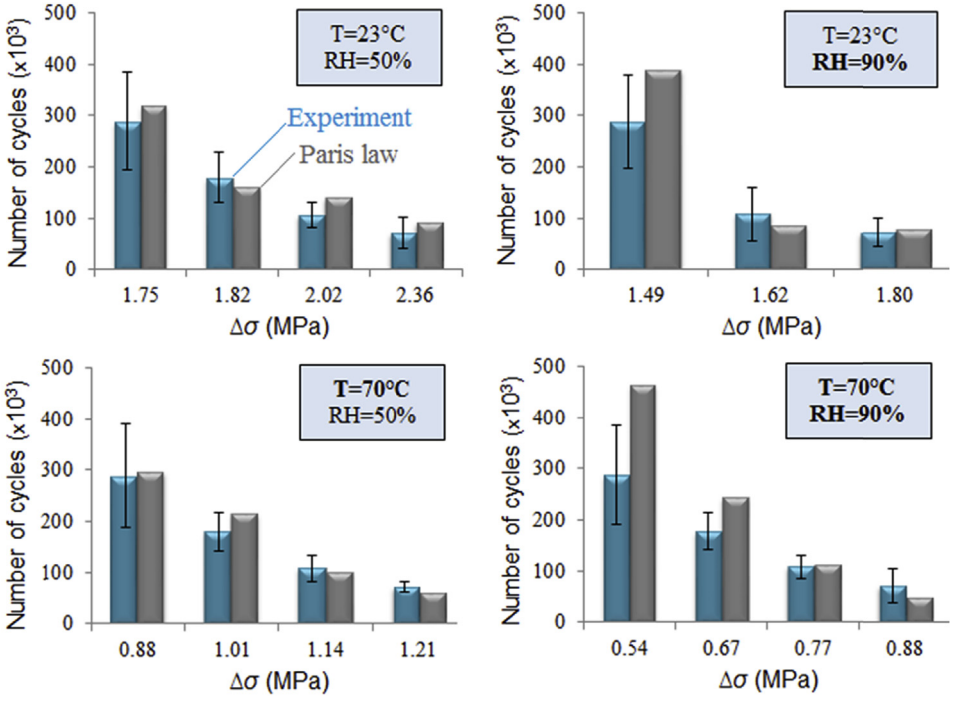

Fig. 8 – Comparison of experimentally measured and semi-analytically calculated (from Paris law) number of fatigue loading cycles applied during various *ex situ* crack propagation test cases conducted on CCM DENT specimens at different stress amplitude ($\Delta\sigma$), temperature (T), and relative humidity (RH) conditions. For graphical clarity, the horizontal axis is not to scale.

analytical crack propagation modelling framework for both pure membranes [26] and CCM composites makes it applicable to either type of CCM treatment during the *in situ* modelling studies.

Conclusions

Quantitative and qualitative aspects of the crack propagation behaviour in the catalyst coated membrane (CCM), which is a core functional component in polymer electrolyte fuel cells, were investigated through a series of *ex situ* uniaxial cyclic tensile experiments conducted on double edge notch tension specimens along with associated microstructural characterization and fracture modelling. The overall trends of the crack growth rates observed in the CCM were generally consistent with those of the pure membrane with respect to the applied stress amplitude, temperature, and humidity, which is suggestive of the dominant role of the membrane on the overall CCM fracture properties. The CCM composite, however, has a higher resistance to elastic deformation and yielding than the pure membrane when subjected to similar tensile forces [37]. Accordingly, the added effect of catalyst layers bonded to the membrane in the CCM composite was found to provide favourable mechanical reinforcement against fracture, which slows down the overall crack propagation rate in the CCM when compared to a pure membrane under similar loads and conditions. Three-dimensional microstructural investigation of the fractured specimens, enabled by X-ray computed tomography, further confirmed that the limiting monolithic crack propagation occurred within the membrane layer of the CCM composite, while the outer catalyst layers developed numerous scattered slender surface cracks ahead of the crack tip, which may have locally compromised their mechanical reinforcement capacity and promoted the crack propagation in this region. While such slender catalyst layer cracks had also developed under pure fatigue conditions independent of any conjoint crack growth, the strong stress concentration effects that accompany crack propagation were found to enhance the severity of these defects. Moreover, localized membrane thinning and interfacial delamination were observed adjacent to the propagating crack tip, which are indicative of the confined yielding effect that accompanies fatigue-driven ductile fracture of the membrane within the CCM composite.

The experimental observations generally indicated that the temperature and humidity variations led to related trends in the fatigue crack propagation behaviour and fundamental mechanical properties of CCM [37]. Accordingly, the time-, temperature-, and humidity-dependent elastic-viscoplastic constitutive mechanical response of CCM composites was first modelled and validated, and then utilized as part of a semi-analytical fracture modelling scheme. A representative model of the *ex situ* crack propagation experiments was simulated using the finite element method (FEM) and its numerical results were utilized in conjunction with analytical fracture mechanics equations and Paris law theory to evaluate the length-wise growth rate of an existing CCM crack as a function of the applied mechanical stress cycles. The results calculated by this integrated semi-analytical fracture modelling framework were in acceptable agreement with the *ex situ* fracture experiments across a range of applied stress, temperature, and humidity conditions that may be experienced by the CCM composite during fuel cell operation. Additionally, the distribution of stress magnitudes and orientations simulated by the FEM model helped explain the various microstructural observations pertaining to the catalyst layer surface defects. The overall effectiveness of the Paris law based semi-analytical fracture modelling framework, as demonstrated for an *ex situ* case for CCM composites in this work, should encourage further application of this methodology to more realistic scenarios transpiring within an operating fuel cell, which can provide useful insights about this critical phenomenon associated directly with the fuel cell durability and lifetime. Given the growing utilization of core-reinforced membranes due to their superior mechanical durability, the characterization and modelling schemes developed in this work could moreover be applied to understand the key aspects of fatigue driven fracture behaviour in reinforced membrane–based CCM composites.

Acknowledgments

This research was supported by Ballard Power Systems and the Natural Sciences and Engineering Research Council (NSERC) of Canada through an Automotive Partnership Canada (APC) grant. We also acknowledge infrastructure funding provided by Canada Foundation for Innovation (CFI) and British Columbia Knowledge Development Fund (BCKDF). The research was undertaken, in part, thanks to funding from the Canada Research Chairs program. We thank Marc-Antoni Goulet for providing tensile test data, and Narinder Singh Khattra for helpful discussions.

REFERENCES

[1] Granovskii M, Dincer I, Rosen MA. Life cycle assessment of hydrogen fuel cell and gasoline vehicles. Int J Hydrogen Energy 2006;31:337–52. https://doi.org/10.1016/j.ijhydene.2005.10.004.
[2] Mench MM. Fuel cell engines. 1st ed. Hoboken, NJ, USA: John Wiley & Sons, Inc.; 2008.
[3] Grebe UD, Nitz LT. 32nd international vienna motor symposium. MTZ Worldw EMagazine 2011;72:64–78.
[4] Kusoglu A, Weber AZ. New insights into perfluorinated sulfonic-acid ionomers. Chem Rev 2017;117:987–1104. https://doi.org/10.1021/acs.chemrev.6b00159.
[5] Mukundan R, Baker AM, Kusoglu A, Beattie P, Knights S, Weber AZ, et al. Membrane accelerated stress test development for polymer electrolyte fuel cell durability validated using field and drive cycle testing. J Electrochem Soc 2018;165:F3085–93. https://doi.org/10.1149/2.0101806jes.
[6] Tavassoli A, Lim C, Kolodziej J, Lauritzen M, Knights S, Wang GG, et al. Effect of catalyst layer defects on local membrane degradation in polymer electrolyte fuel cells. J Power Sources 2016;322:17–25.

[7] Gittleman CS, Coms FD, Lai YH. Membrane durability: physical and chemical degradation. In: Mench M, Kumbur EC, Veziroglu TN, editors. Polym. Electrolyte fuel cell degrad. Cambridge MA: Academic Press; 2012. p. 15–88.
[8] Kreitmeier S, Schuler GA, Wokaun A, Büchi FN. Investigation of membrane degradation in polymer electrolyte fuel cells using local gas permeation analysis. J Power Sources 2012;212:139–47. https://doi.org/10.1016/j.jpowsour.2012.03.071.
[9] Moor G De, Bas C, Charvin N, Dillet J, Maranzana G, Haye D, et al. Perfluorosulfonic acid membrane degradation in the hydrogen inlet region: a macroscopic approach. Int J Hydrogen Energy 2015;41:483–96. https://doi.org/10.1016/j.ijhydene.2015.10.066.
[10] Alavijeh AS, Khorasany RMH, Nunn Z, Habisch A, Lauritzen M, Rogers E, et al. Microstructural and mechanical characterization of catalyst coated membranes subjected to in situ hygrothermal fatigue. J Electrochem Soc 2015;162:1461–9. https://doi.org/10.1149/2.0471514jes.
[11] Ghassemzadeh L, Holdcroft S. Quantifying the structural changes of perfluorosulfonated acid ionomer upon reaction with hydroxyl radicals. J Am Chem Soc 2013;135:8181–4.
[12] Ghassemzadeh L, Peckham TJ, Weissbach T, Luo X, Holdcroft S. Selective formation of hydrogen and hydroxyl radicals by electron beam irradiation and their reactivity with perfluorosulfonated acid ionomer. J Am Chem Soc 2013;135:15923–32.
[13] Danilczuk M, Coms FD, Schlick S. Visualizing chemical reactions and crossover processes in a fuel cell inserted in the ESR resonator: detection by spin trapping of oxygen radicals, nafion-derived fragments, and hydrogen and deuterium atoms. J Phys Chem B 2009;113:8031.
[14] Sadeghi Alavijeh A, Goulet M-A, Khorsany R, Ghataurah J, Lim C, Lauritzen M, et al. Decay in mechanical properties of catalyst coated membranes subjected to combined chemical and mechanical membrane degradation. Fuel Cells 2015;15:204–13.
[15] Lim C, Ghassemzadeh L, Van Hove F, Lauritzen M, Kolodziej J, Wang GGG, et al. Membrane degradation during combined chemical and mechanical accelerated stress testing of polymer electrolyte fuel cells. J Power Sources 2014;257:102–10.
[16] Huang X, Solasi R, Zou YUE, Feshler M, Reifsnider K, Condit D, et al. Mechanical endurance of polymer electrolyte membrane and PEM fuel cell durability. J Polym Sci B Polym Phys 2006;44:2346–57. https://doi.org/10.1002/polb.
[17] Luo X, Ghassemzadeh L, Holdcroft S. Effect of free radical-induced degradation on water permeation through PFSA ionomer membranes. Int J Hydrogen Energy 2015;40:16714–23. https://doi.org/10.1016/j.ijhydene.2015.07.118.
[18] Khorasany RMH, Singh Y, Sadeghi Alavijeh A, Kjeang E, Wang GG, Rajapakse RKND. Fatigue properties of catalyst coated membranes for fuel cells: ex-situ measurements supported by numerical simulations. Int J Hydrogen Energy 2016;41:8992–9003.
[19] Khorasany RMH, Sadeghi Alavijeh A, Kjeang E, Wang GG, Rajapakse RKND. Mechanical degradation of fuel cell membranes under fatigue fracture tests. J Power Sources 2015;274:1208–16.
[20] Kusoglu A, Santare MH, Karlsson AM. Aspects of fatigue failure mechanisms in polymer fuel cell membranes. J Polym Sci, Part B: Polym Phys 2011;49:1506–17. https://doi.org/10.1002/polb.22336.
[21] Sadeghi Alavijeh A, Khorasany RMH, Habisch A, Wang GG, Kjeang E. Creep properties of catalyst coated membrane in polymer electrolyte fuel cells. J Power Sources 2015;285:16–28.
[22] Sadeghi Alavijeh A, Venkatesan SV, Khorasany RMH, Kim WHJ, Kjeang E. Ex-situ tensile fatigue-creep testing: a powerful tool to simulate in-situ mechanical degradation in fuel cells. J Power Sources 2016;312:123–7.
[23] Kusoglu A, Calabrese M, Weber AZ. Effect of mechanical compression on chemical degradation of nafion membranes. ECS Electrochem Lett 2014;3:F33–6. https://doi.org/10.1149/2.008405eel.
[24] Yoon W, Huang X. Acceleration of chemical degradation of perfluorosulfonic acid ionomer membrane by mechanical stress: experimental evidence. ECS Trans 2010;33:907–11. https://doi.org/10.1149/1.3484584.
[25] Kreitmeier S, Lerch P, Wokaun A, Büchi FN. Local degradation at membrane defects in polymer electrolyte fuel cells. J Electrochem Soc 2013;160:F456–63. https://doi.org/10.1149/1.023306jes.
[26] Singh Y, Khorasany RMH, Sadeghi Alavijeh A, Kjeang E, Wang GG, Rajapakse RKND. Ex situ measurement and modelling of crack propagation in fuel cell membranes under mechanical fatigue loading. Int J Hydrogen Energy 2017;42:19257–71.
[27] Zhang J, Tang Y, Song C, Zhang J, Wang H. PEM fuel cell open circuit voltage (OCV) in the temperature range of 23 °C to 120 °C. J Power Sources 2006;163:532–7. https://doi.org/10.1016/j.jpowsour.2006.09.026.
[28] Zatoń M, Rozière J, Jones DJ. Current understanding of chemical degradation mechanisms of perfluorosulfonic acid membranes and their mitigation strategies: a review. Sustain Energy Fuels 2017;1:409–38. https://doi.org/10.1039/C7SE00038C.
[29] Majsztrik PW, Bocarsly AB, Benziger JB. Viscoelastic response of nafion . Effects of temperature and hydration on tensile creep. Macromolecules 2008;41:9849–62.
[30] Safronova E, Golubenko D, Pourcelly G, Yaroslavtsev A. Mechanical properties and influence of straining on ion conductivity of perfluorosulfonic acid Nafion®-type membranes depending on water uptake. J Membr Sci 2015;473:218–25.
[31] Osborn SJ, Hassan MK, Divoux GM, Rhoades DW, Mauritz KA, Moore RB. Glass transition temperature of perfluorosulfonic acid ionomers. Macromolecules 2007;40:3886–90.
[32] Matos BR, Dresch MA, Santiago EI, Linardi M, de Florio DZ, Fonseca FC. Nafion -relaxation dependence on temperature and relative humidity studied by dielectric spectroscopy. J Electrochem Soc 2012;160:F43–8.
[33] Kusoglu A, Tang Y, Santare MH, Karlsson AM, Cleghorn S, Johnson WB. Stress-strain behavior of perfluorosulfonic acid membranes at various temperatures and humidities: experiments and phenomenological modeling. J Fuel Cell Sci Technol 2009;6. 0110121–8.
[34] Kusoglu A, Tang Y, Lugo M, Karlsson AM, Santare MH, Cleghorn S, et al. Constitutive response and mechanical properties of PFSA membranes in liquid water. J Power Sources 2010;195:483–92.
[35] Silberstein MN, Boyce MC. Constitutive modeling of the rate, temperature, and hydration dependent deformation response of Nafion to monotonic and cyclic loading. J Power Sources 2010;195:5692–706.
[36] Silberstein MN, Pillai PV, Boyce MC. Biaxial elastic–viscoplastic behavior of Nafion membranes. Polymer 2011;52:529–39.
[37] Goulet MA, Khorasany RMH, De Torres C, Lauritzen M, Kjeang E, Wang GG, et al. Mechanical properties of catalyst coated membranes for fuel cells. J Power Sources 2013;234:38–47.
[38] Satterfield MB, Benziger JB. Non-fickian water vapor sorption dynamics by nafion membranes. J Phys Chem B 2008;112:3693–704.

[39] Goulet M, Arbour S, Lauritzen M, Kjeang E. Water sorption and expansion of an ionomer membrane constrained by fuel cell electrodes. J Power Sources 2015;274:94–100.
[40] Lai Y-H, Mittelsteadt CK, Gittleman CS, Dillard DA. Viscoelastic stress analysis of constrained proton exchange membranes under humidity cycling. J Fuel Cell Sci Technol 2009;6. 021002.
[41] Panha K, Fowler M, Yuan XZ, Wang H. Accelerated durability testing via reactants relative humidity cycling on PEM fuel cells. Appl Energy 2012;93:90–7.
[42] Singh Y, White RT, Najm M, Haddow T, Pan V, Orfino FP, et al. Tracking the evolution of mechanical degradation in fuel cell membranes using 4D in situ visualization. J Power Sources 2019;412:224–37. https://doi.org/10.1016/j.jpowsour.2018.11.049.
[43] Kang J, Kim J. Membrane electrode assembly degradation by dry/wet gas on a PEM fuel cell. Int J Hydrogen Energy 2010;35:13125–30.
[44] Zhang S, Yuan X, Wang H, Merida W, Zhu H, Shen J, et al. A review of accelerated stress tests of MEA durability in PEM fuel cells. Int J Hydrogen Energy 2009;34:388–404. https://doi.org/10.1016/j.ijhydene.2008.10.012.
[45] Macauley N, Sadeghi Alavijeh A, Watson M, Kolodziej J, Knights S, Wang G, et al. Accelerated membrane durability testing of heavy duty fuel cells. J Electrochem Soc 2015;162:F98–107.
[46] Singh Y, Orfino FP, Dutta M, Kjeang E. 3D visualization of membrane failures in fuel cells. J Power Sources 2017;345:1–11.
[47] Singh Y, Orfino FP, Dutta M, Kjeang E. 3D failure analysis of pure mechanical and pure chemical degradation in fuel cell membranes. J Electrochem Soc 2017;164:F1331–41.
[48] Ramani D, Singh Y, Orfino FP, Dutta M, Kjeang E. Characterization of membrane degradation growth in fuel cells using X-ray computed tomography. J Electrochem Soc 2018;165:F3200–8. https://doi.org/10.1149/2.0251806jes.
[49] Aindow TT, O'Neill J. Use of mechanical tests to predict durability of polymer fuel cell membranes under humidity cycling. J Power Sources 2011;196:3851–4.
[50] Pestrak M, Li Y, Case SW, Dillard D a, Ellis MW, Lai Y-H, et al. The effect of mechanical fatigue on the lifetimes of membrane electrode assemblies. J Fuel Cell Sci Technol 2010;7. 041009.
[51] Khorasany RMH, Sadeghi Alavijeh A, Kjeang E, Wang GG, Rajapakse RKND. Simulation of ionomer membrane fatigue under mechanical and hygrothermal loading conditions. J Power Sources 2015;279:55–63.
[52] Khorasany RMH, Singh Y, Sadeghi Alavijeh A, Rajapakse RKND, Kjeang E. In-situ simulation of membrane fatigue in polymer electrolyte fuel cells. Int J Hydrogen Energy 2017;42:11838–44.
[53] Tang H, Pan M, Wang F, Shen PK, Jiang SP. Highly durable proton exchange membranes for low temperature fuel cells. J Phys Chem B 2007;111:8684–90.
[54] Crum M, Liu W. Effective testing matrix for studying membrane durability in PEM fuel cells: Part 2. Mechanical durability and combined mechanical and chemical durability. Electrochem Soc Trans 2006;3:541–50.
[55] Lim C, Sadeghi Alavijeh A, Lauritzen M, Kolodziej J, Knights S, Kjeang E. Fuel cell durability enhancement with cerium oxide under combined chemical and mechanical membrane degradation. ECS Electrochem Lett 2015;4:F29–31.
[56] Macauley N, Ghassemzadeh L, Lim C, Watson M, Kolodziej J, Lauritzen M, et al. Pt band formation enhances the stability of fuel cell membranes. ECS Electrochem Lett 2013;2:F33–5.
[57] Wong KH, Kjeang E. Mitigation of chemical membrane degradation in fuel cells: understanding the effect of cell voltage and iron ion redox cycle. ChemSusChem 2015;8:1072–82.
[58] Poornesh KK, Sohn Y-J, Park G-G, Yang T-H. Gas-diffusion layer's structural anisotropy induced localized instability of nafion membrane in polymer electrolyte fuel cell. Int J Hydrogen Energy 2012;37:15339–49. https://doi.org/10.1016/j.ijhydene.2012.04.154.
[59] Li Y, Quincy JK, Case SW, Ellis MW, Dillard DA, Lai Y. Characterizing the fracture resistance of proton exchange membranes. J Power Sources 2008;185:374–80.
[60] Moukheiber E, Bas C, Flandin L. Understanding the formation of pinholes in PFSA membranes with the essential work of fracture (EWF). Int J Hydrogen Energy 2014;39:2717–23. https://doi.org/10.1016/j.ijhydene.2013.03.031.
[61] Jia R, Dong S, Hasegawa T, Ye J, Dauskardt RH. Contamination and moisture absorption effects on the mechanical properties of catalyst coated membranes in PEM fuel cells. Int J Hydrogen Energy 2012;37:6790–7. https://doi.org/10.1016/j.ijhydene.2012.01.063.
[62] Patankar K, Dillard DA, Case SW, Ellis MW, Li Y, Lai Y. Characterizing fracture energy of proton exchange membranes using a knife slit test. J Polym Sci Part B Polym Chem 2010;48:333–43.
[63] Zhang Z, Shi S, Lin Q, Wang L, Liu Z, Li P, et al. Exploring the role of reinforcement in controlling fatigue crack propagation behavior of perfluorosulfonic-acid membranes. Int J Hydrogen Energy 2018;43:6379–89. https://doi.org/10.1016/j.ijhydene.2018.02.034.
[64] Lin Q, Shi S, Wang L, Chen X, Chen G. Biaxial fatigue crack propagation behavior of perfluorosulfonic-acid membranes. J Power Sources 2018;384:58–65. https://doi.org/10.1016/j.jpowsour.2018.02.002.
[65] Li Y, Dillard DA, Case SW, Ellis MW, Lai YH, Gittleman CS, et al. Fatigue and creep to leak tests of proton exchange membranes using pressure-loaded blisters. J Power Sources 2009;194:873–9. https://doi.org/10.1016/j.jpowsour.2009.06.083.
[66] Hu M, Cao G. Research on the long-term stability of a PEMFC stack: analysis of pinhole evolution. Int J Hydrogen Energy 2014;39:7940–54. https://doi.org/10.1016/j.ijhydene.2014.03.072.
[67] Theiler A, Karpenko-jereb L. Modelling of the mechanical durability of constrained Nafion membrane under humidity cycling. Int J Hydrogen Energy 2015;40:9773–82.
[68] Kusoglu A, Weber AZ. A mechanistic model for pinhole growth in fuel-cell membranes during cyclic loads. J Electrochem Soc 2014;161:E3311–22. https://doi.org/10.1149/2.036408jes.
[69] Banan R, Bazylak A, Zu J. Effect of mechanical vibrations on damage propagation in polymer electrolyte membrane fuel cells. Int J Hydrogen Energy 2013;38:14764–72.
[70] Banan R, Zu J, Bazylak A. Humidity and temperature cycling effects on cracks and delaminations in PEMFCs. Fuel Cells 2015;15(2):327–36.
[71] Banan R, Bazylak A, Zu J. Combined effects of environmental vibrations and hygrothermal fatigue on mechanical damage in PEM fuel cells. Int J Hydrogen Energy 2015;40:1911–22.
[72] Ding G, Santare MH, Karlsson AM, Kusoglu A. Numerical evaluation of crack growth in polymer electrolyte fuel cell membranes based on plastically dissipated energy. J Power Sources 2016;316:114–23.
[73] Paris PC, Gomez MP, Anderson WE. A rational analytic theory of fatigue. Trend Eng 1961;13:9–14.
[74] Khorasany RMH, Goulet MA, Sadeghi Alavijeh A, Kjeang E, Wang GG, Rajapakse RKND. On the constitutive relations for catalyst coated membrane applied to in-situ fuel cell modeling. J Power Sources 2014;252:176–88.

[75] Pommier S, Gravouil A. Extended finite element method for crack propagation. 1st ed. London, UK: ISTE; 2011.
[76] Goulet MA, Khorasany RMH, De Torres C, Lauritzen M, Kjeang E, Wang GG, et al. Mechanical properties of catalyst coated membranes for fuel cells. J Power Sources 2013;234:38–47. https://doi.org/10.1016/j.jpowsour.2013.01.128.
[77] Kai Y, Kitayama Y, Omiya M, Uchiyama T, Kato M. Crack formation in membrane electrode assembly under static and cyclic loadings. J Fuel Cell Sci Technol 2013;10.021007.
[78] Kundu S, Fowler MW, Simon LC, Grot S. Morphological features (defects) in fuel cell membrane electrode assemblies. J Power Sources 2006;157:650–6.
[79] Lu Z, Santare MH, Karlsson AM, Busby FC, Walsh P. Time-dependent mechanical behavior of proton exchange membrane fuel cell electrodes. J Power Sources 2014;245:543–52. https://doi.org/10.1016/j.jpowsour.2013.07.013.
[80] Khan SU, Alderliesten RC, Benedictus R. Post-stretching induced stress redistribution in Fibre Metal Laminates for increased fatigue crack growth resistance. Compos Sci Technol 2009;69:396–405. https://doi.org/10.1016/j.compscitech.2008.11.006.
[81] Yoon W, Huang X. A nonlinear viscoelastic–viscoplastic constitutive model for ionomer membranes in polymer electrolyte membrane fuel cells. J Power Sources 2011;196:3933–41.
[82] Bergström JS, Boyce MC. Large strain time-dependent behavior of filled elastomers. Mech Mater 2000;32:627–44.
[83] Ragab A-R, Bayoumi SE. Engineering solid mechanics: fundamentals and applications. Boca Raton (FL): CRC Press LLC; 1999.
[84] Tada H, Paris PC, Irwin GR. The stress analysis of cracks handbook. 2nd ed. Paris Productions &: Del Research Corp.); 1985.
[85] Mohammadi S. Extended finite element method for fracture analysis of structures. Malden (MA): Blackwell; 2008.
[86] Joshi AY, Sharma SC, Harsha SP. Analysis of crack propagation in fixed-free single-walled carbon nanotube under tensile loading using XFEM. J Nanotechnol Eng Med 2010;1. 041008.
[87] Khattra NS, Lu Z, Karlsson AM, Santare MH, Busby FC, Schmiedel T. Time-dependent mechanical response of a composite PFSA membrane. J Power Sources 2013;228:256–69. https://doi.org/10.1016/j.jpowsour.2012.11.116.
[88] Khattra NS, Karlsson AM, Santare MH, Walsh P, Busby FC. Effect of time-dependent material properties on the mechanical behavior of PFSA membranes subjected to humidity cycling. J Power Sources 2012;214:365–76. https://doi.org/10.1016/j.jpowsour.2012.04.065.